Clim Dyn
DOI 10.1007/s00382-013-2002-7

Future change of the Indian Ocean basin-wide and dipole modes in the CMIP5

Jung-Eun Chu · Kyung-Ja Ha · June-Yi Lee · Bin Wang · Byeong-Hee Kim · Chul Eddy Chung

Received: 19 March 2013 / Accepted: 23 September 2013

Abstract The Indian Ocean sea surface temperature (SST) variability has been represented with the two dominant variability modes: the Indian Ocean basin-wide (IOBW) and dipole (IOD) modes. Here we investigate future changes of the two modes together with mean state and El Niño and Southern Oscillation (ENSO) relationship under the anthropogenic global warming using 20 coupled models that participated in the phase five of Coupled Model Intercomparison Project by comparing the historical run from 1950 to 2005 and the RCP 4.5 run from 2050 to 2099. The five best models are selected based on the evaluation of the 20 models' performances in simulating the two modes and Indian Ocean basic state for the latest 56 years. They are capable of capturing the IOBW and IOD modes in their spatial distribution, seasonal cycle, major periodicity, and relationship with ENSO to some extent. The five best models project the significant changes in the Indian Ocean mean state and variability including the two dominant modes in the latter part of twenty-first century under the anthropogenic warming scenario. First, the annual mean climatological SST displays an IOD-like pattern change over the Indian Ocean with enhanced warming in the northwestern Indian Ocean and relatively weaker warming off the Sumatra–Java coast. It is also noted that the monthly SST variance is increased over the eastern and southwestern Indian Ocean. Second, the IOBW variability on a quasi-biennial time scale will be enhanced due to the strengthening of the ENSO–IOBW mode relationship although the total variance of the IOBW mode will be significantly reduced particularly during late summer and fall. The enhanced air-sea coupling over the Indian-western Pacific climate in response to El Nino activity in the future projection makes favorable condition for a positive IOD while it tends to derive relatively cold temperature over the eastern Indian Ocean. This positive IOD-like ENSO response weakens the relationship between the eastern Indian Ocean and El Nino while strengthens the relationship with western Indian Ocean. Third, the IOD mode, intrinsic coupled mode of the Indian Ocean may not be changed appreciably under the anthropogenic global warming.

Keywords Global warming · Indian Ocean · SST · Indian Ocean basin-wide (IOBW) · Indian Ocean dipole (IOD) · CMIP5 · ENSO

J.-E. Chu · K.-J. Ha · J.-Y. Lee (✉) · B.-H. Kim
Pusan National University, Busandaehak-ro 63beon-gil, Geumjeong-gu, Busan 609-735, Korea
e-mail: juneyi@pusan.ac.kr

B. Wang
International Pacific Research Center, University of Hawaii, Honolulu, HI 96822, USA

B. Wang
Department of Meteorology, University of Hawaii, Honolulu, HI 96833, USA

C. E. Chung
Gwangju Institute of Science and Technology (GIST), Kwangju 500-712, Korea

1 Introduction

The Indian Ocean is a part of large warm water pool and neighboring the great monsoons of Asia that anchor the major convection center of the atmosphere (Saji et al. 2006). It has been recognized that the variability and changes of the Indian Ocean sea surface temperature (SST) play an important role in climate variability worldwide including Asian summer monsoon (e.g., Abram et al. 2008;

Published online: 29 November 2013

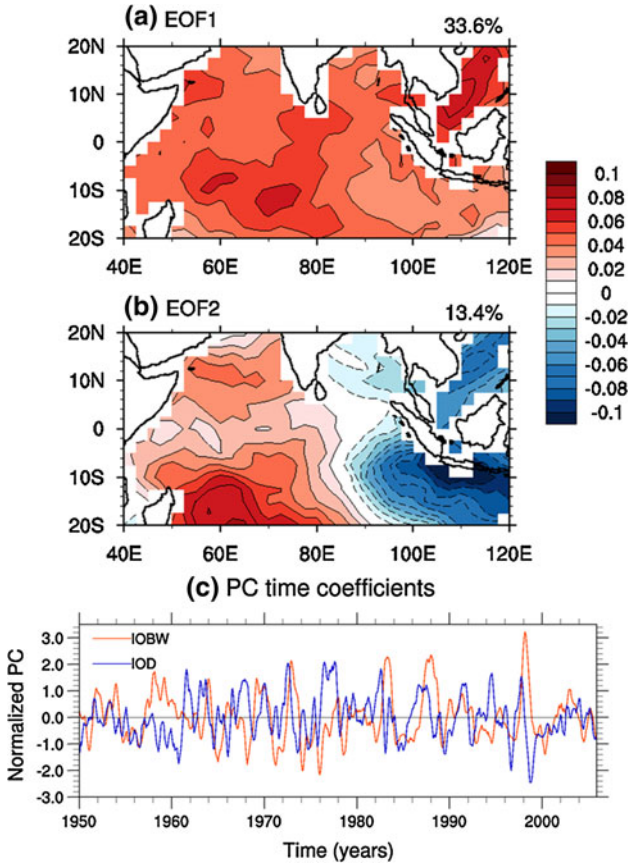

Fig. 1 Spatial patterns of (**a**) the first and the (**b**) second EOF modes of the observed monthly SST anomalies over the Indian Ocean (20°S–20°N, 40°–120°E). Monthly linear trends are removed based on the period from 1950 to 2005

Schott et al. 2009), Northwestern Pacific climate (e.g., Chowdary et al. 2010; Xie et al. 2009), the African Sahel drying trend (e.g., Giannini et al. 2003), and El Niño and Southern Oscillation (ENSO) (e.g. Yu et al. 2002; Luo et al. 2012). The major modes of change/variability of the Indian Ocean SST include the basin-wide mode, and dipole mode (Fig. 1). The Indian Ocean basin-wide (IOBW) variability mode is characterized by a basin-wide warming or cooling with about 3-year period. The fact that the IOBW, peaking in early spring, tends to follow by the mature phase of ENSO suggests that the ENSO remote forcing is a crucial factor in the IOBW (Saji and Yamagata 2003; Latif and Barnett 1995). The Indian Ocean dipole (IOD) mode is an intrinsic mode of Indian ocean–atmosphere coupled system and tends to have a biennial frequency (Saji et al. 1999; Webster et al. 1999).

Recent studies have found significant warming and changes in the Indian Ocean SST during recent few decades based on observation (Abram et al. 2008; Alory et al. 2007; Chowdary et al. 2012; Ihara et al. 2008). Ihara et al. (2008) showed that the western equatorial Indian Ocean warms more than the eastern counterpart during recent decades; the mean SST gradient across the equatorial Indian Ocean is anomalously positive to the west reduced. This differential heating is related to a persistent shoaling of the thermocline in the eastern equatorial Indian Ocean (Alory et al. 2007; Tokinaga et al. 2012), which in turn leads to strengthening of IOD by enhancing thermocline feedback during recent few decades (Abram et al. 2008). Chowdary et al. (2012) argued that there is decadal variability of the relationship between ENSO and Indo-western Pacific climate and the range is not outside of natural variability based on long-term ship-based observation. The Indian Ocean SST variability under global warming have also explored through climate change projections (Du and Xie 2008; Meehl et al. 2007a, b; Saji et al. 2006; Vecchi and Soden 2007). Saji et al. (2006) have found that a majority of the models that submitted to the Intergovernmental Panel on Climate Change's Fourth Assessment Report (IPCC AR4) successes to appear the mean state of the equatorial Indian Ocean and the success in representation of the mean states enables to display an equatorial zonal mode with spatial structure and seasonality similar to the IOD. The response of the Indian Ocean to global warming resembled the positive phase of IOD events (Vecchi and Soden 2007), but IOD activity does not intensified in spite of enhanced thermocline feedback since the cancelling out with weakened atmospheric feedback (Zheng et al. 2010, 2013).

The dynamical linkage between the Indian Ocean and Pacific Ocean through atmospheric circulation is still controversial issues. Several studies suggested that the warming trend in the tropical Indian Ocean is likely associated with the observed weakening of the Pacific trade winds (i.e. weakening of Walker circulation) and transmitted to the Indian Ocean thermocline by Indonesian throughflow (Alory et al. 2007; Tokinaga et al. 2012; Vecchi and Soden 2007). On the other hand, recent evidence based on high-quality observations suggested that the tropical Pacific trade winds may have actually strengthened over the past two decades emphasizing the role of Indian Ocean warming relative to the Pacific's in modulating the Pacific climate changes in the twenty-first centuries (Luo et al. 2012). Several recent studies have actively discussed how ENSO (e.g. Kim and Yu 2012) or monsoon precipitation (e.g. Hsu and Li 2012; Lee and Wang 2012; Wang et al. 2013) would change under global warming using the third and phase five of the Coupled Model Intercomparison Project (CMIP3 and CMIP5) projections.

Until now, several studies have looked at the future changes in IOD variability or linkage between the Indian Ocean and Pacific Ocean, separately. Evaluation of the CMIP5 models in simulating the IOBW mode in present

climate has also attempted in terms of capacitor effect of Indian Ocean SST (Du at el. 2013). However, future changes in both IOBW and IOD variability in the CMIP5 projection and their evaluation have not been attempted. Therefore, this study investigates the future changes of the IOBW, and IOD modes projected by the 20 coupled atmosphere–ocean models (CGCMs) that participated in the CMIP5 by comparing two runs: the historical run under changing solar-volcanic forcing and anthropogenic influences from 1850 to 2005 and the Representative Concentration Pathway (RCP) 4.5 run assuming that radiative forcing will stabilize with an increases of about 4.5 Wm^{-2} after 2100 (Taylor et al. 2012). In addition, evaluation of models' historical simulations and estimation of uncertainty in the corresponding future projections are crucial steps for the assessment of the future changes. These will be carefully examined in the present study. Detailed description of the model and data used is given in Sect. 2. Section 3 evaluates historical simulations of the 20 coupled models against the observation for the period of 1950 to 2005. Future change of the Indian Ocean and ENSO-Indian Ocean relationship is discussed in Sect. 4, respectively. Section 5 summarizes the results.

2 Model and data

2.1 Models and experiments

Total 20 CGCMs participated in CMIP5 are used in this study. Table 1 lists the model name, institution and horizontal resolution of atmospheric component. Two experiments are investigated. One is the historical run (i.e., the twentieth century run) from 1850 to 2005 and the other is the RCP 4.5 run from 2006 to 2100. The historical run was imposed changing conditions consistent with observations which may include atmospheric composition (including CO_2) due to both anthropogenic and volcanic influences, solar forcing, emissions or concentrations of short-lived species and natural and anthropogenic aerosols or their precursors, and land use. The RCP4.5 run assumes that radiative forcing will increase and then stabilize at about 4.5 Wm^{-2} after 2100 and is chosen as a "central" scenario in CMIP5 (Taylor et al. 2012).

Seven models (CanESM2, GFDL-ESM2 M, HadGEM2-CC, HadGEM2-ES, MIROC-ESM, MPI-ESM, and Nor-ESM1-M) in the CMIP5 are Earth System Models (ESM). They include bio-geochemical components that account for the important fluxes of carbon between the ocean, atmosphere, and terrestrial biosphere carbon reservoirs and may in some cases include interactive prognostic aerosol, chemistry, and dynamical vegetation components (Taylor et al. 2012). Thus, CMIP5 models may have larger response to natural forcing and aerosols than CMIP3 CGCMs (Yeh et al. 2012). Some of CMIP5 CGCMs perform simulations with a higher resolution or a more complete treatment of atmospheric chemistry than CMIP3 CGCMs. One can find detailed information on CMIP5 models and experiments at http://cmip-pcmdi.llnl.gov/cmip5/experiment_design.html and some related papers (e.g., Taylor et al. 2012).

In general, the CMIP5 CGCMs have a larger number of ensemble simulations for the historical run than for the RCP4.5 run. For more fair comparison, we use the same number of ensemble members for the two runs in individual models. Table 1 shows the number of ensemble members used for each model. To validate the CGCMs in their historical simulations with respect to observation, each model run was interpolated to a common 2.5° lat × 2.5° lon grid. To get the mean characteristics of individual models, the multi-model mean (MMM) analysis was constructed using equal weighted mean of individual model's climatology, monthly variance. For the purpose of empirical orthogonal function (EOF) analysis, consecutive multi model (CMM) analysis is applied rather than MMM analysis. The CMM analysis is a method to consecutively piece together the individual models. The climatology was obtained for the 56 years of 1950–2005.

2.2 Observation

The observed SST is obtained from the Hadley Centre SST dataset (HadISST, Rayner et al. 2003). All observed data were interpolated to a common 2.5° lat × 2.5° lon grid. Same as the model data, observed climatology was obtained for the 56 years of 1950–2005. As a basic reference of large-scale circulation change including wind and geopotential height, National Centers for Environmental Prediction–National Center for Atmospheric Research (NCEP–NCAR) reanalysis is used (Kalnay 1996).

3 Evaluation of historical runs

Prior to the estimation of future projections, we assess the 20 CMIP5 CGCMs in simulating climatology and variability of the Indian Ocean SST during the historical run period of 1950–2005. This is crucial steps to understand current states of climate projection in representing dominant variability of the Indian Ocean. The evaluation metrics includes (1) the annual mean of SST climatology, (2) monthly variance of SST, (3) the IOBW mode, and (4) the IOD mode. Taking into account the significant inter-model spread over their MMM, several models will be selected in Sect. 3.4 assuming that best model in simulating Indian Ocean SST variability is the model which realistically

Table 1 Description of CMIP5 models used in the study

Coupled model	Institution	AGCM resolution	Ens no.
ACCESS1-0	Commonwealth Scientific and Industrial Research Organisation and Bureau of Meteorology, Australia (CSIRO–BOM)	1.875° × 1.25°	1
BCC-CSM1.1	Beijing Climate Center, China Meteorological Administration (BCC)	2.8125° × 2.8125°	1
CanESM2	Canadian Centre for Climate Modelling and Analysis (CCCma)	2.8125° × 2.8125°	5
CCSM4	National Center for Atmospheric Research (NCAR)	1.25° × 0.9375°	1
CNRM-CM5	Centre National de Recherches Meteorologiques/Centre Europeen de Recherche et Formation Avancees en Calcul Scientifique (CNRM-CERFACS)	1.40625° × 11.40625°	1
CSIRO-Mk3-6-0	Commonwealth Scientific and Industrial Research Organisation and the Queensland Climate Change Centre of Excellence (CSIRO–QCCCE)	1.875° × 1.875°	3
FGOALS-g2	LASG, Institute of Atmospheric Physics, Chinease Academy of Sciences; and CESS, Tsinghua University (LASG–CESS)	2.8125° × 2.8125°	1
GFDL-CM3	Geophysical Fluid Dynamics Laboratory (NOAA GFDL)	2.5° × 2°	1
GFDL-ESM2 M		2.5° × 2°	1
GISS-E2-R	NASA Goddard Institute for Space Studies (NASA GISS)	2.5° × 2°	2
HadGEM2-CC	Met Office Hadley Centre (MOHC)	1.875° × 1.24°	1
HadGEM2-ES		1.875° × 1.24°	1
INM-CM4	Institute for Numerical Mathematics (INM)	2° × 1.5°	1
IPSL-CM5A-LR	Institute Pierre-Simon Laplace (IPSL)	3.75° × 1.875°	4
IPSL-CM5A-MR		2.5° × 1.258°	
MIROC5	Atmosphere and Ocean Research Institute (University of Tokyo), National Institute for Environmental Studies, and Japan Agency for Marine-Earth Science and Technology (MIROC)	1.40625° × 1.40625°	1
MIROC-ESM		2.8125° × 2.8125°	1
MPI-ESM-LR	Max Planck Institute for Meteorology (MPI-M)	1.875°× 1.875°	3
MRI-CGCM3	Meteorological Research Institute (MRI)	1.125° × 2.25°	1
NorESM1-M	Norwegian Climate Centre (NCC)	2.5° × 1.875°	1

represent annual mean climatology, monthly variance, and two leading modes together.

3.1 Annual mean of SST climatology

On average, annual mean climatological SST over the Indian Ocean is 27.5 °C in which equatorial eastern Indian Ocean is warmer then western Indian Ocean (Fig. 2a). The 20 CGCM's MMM realistically reproduces the observed features (Fig. 2b). The pattern correlation coefficient (PCC) between the observation and simulation reaches 0.95. A difference map (not shown) indicates that MMM tends to underestimate annual mean SST climatology over the entire Indian Ocean. The averaged bias is −0.37 °C with larger value over the northern Indian Ocean.

To objectively evaluate the model's performance, we calculate the PCC and normalized standard deviation in terms of Taylor diagram (Fig. 3a). The normalized standard deviation is the ratio of individual model's spatial standard deviation divided by the observed spatial standard deviation over the tropical Indian Ocean region of 20°S–20°N, 40°–120°E. The individual model's PCC range from 0.60 to 0.97 and normalized standard deviation ranges from 0.78 to 1.71 (Fig. 3a). The MMM is evidently better than individual models in simulating annual mean SST climatology with PCC of 0.95 and the normalized standard deviation of 1.04.

3.2 Variance of monthly SST

The spatial pattern of the variance of monthly SST shows that larger variance over the region close to land area because of freshwater fluxes from a variety of sources including the Indonesian throughflow, heavy oceanic precipitation, and river runoff from adjacent land regions (Fig. 2c). In addition to annual mean of SST climatology, the 20 CGCM's MMM well reproduces the observed features of variance of monthly SST (Fig. 2d). The PCC between the observation and simulation is 0.86 which is less than that of annual meal climatology but still significantly high. The MMM tends to overestimate the variance of monthly SST variability over the eastern Indian Ocean and underestimate over the western Indian Ocean (not shown). Comparing to annual mean climatology, the monthly variance has widely spread distribution of normalized standard

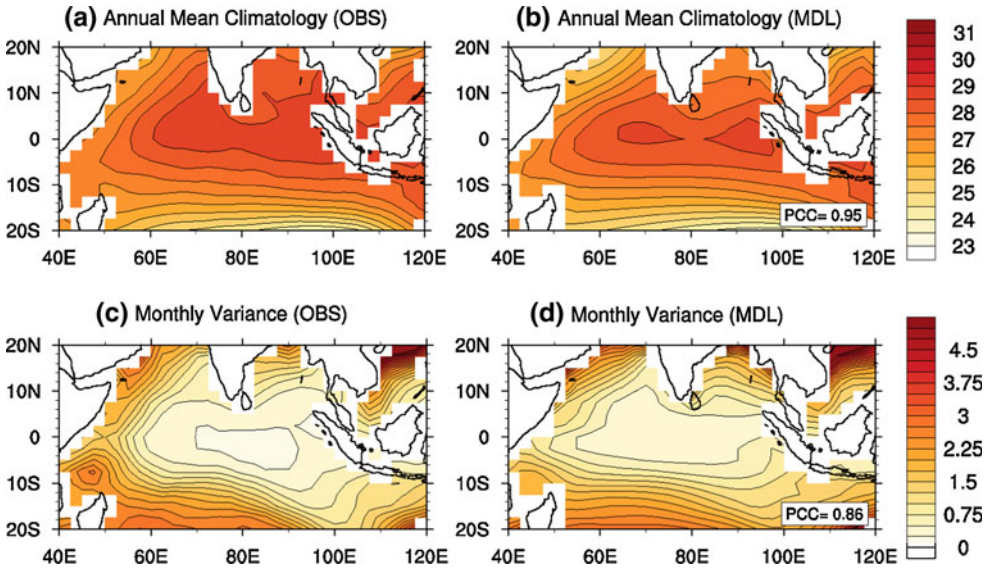

Fig. 2 Annual mean SST climatology (°C) (**a**, **b**) and variance of monthly SST (**c**, **d**) for observation (*left*) and model (*right*) from 1950 to 2005 over the Indian Ocean (20°S–20°N, 40°–120°E). The *numbers* in the *right lower corners* indicate pattern correlation coefficient (*PCC*) between the observed and simulated patterns

deviation which range from 0.89 to 2.66 (Fig. 3b). The individual model's PCC ranges from 0.49 to 0.89. The MMM has better skill than individual models in simulating the monthly variance with PCC of 0.86 and the normalized standard deviation of 1.33. It is noted that the MPI-ESM-LR is the best model to reproduces the annual mean and monthly variance of the Indian Ocean SST. It has been suggested that the model that has a realistic simulation of the mean field tends to have better simulation of variability (e.g., Lee et al 2010)

3.3 The leading modes

To obtain the major modes of the observed Indian Ocean SST variability, we apply EOF analysis on monthly SST anomaly that was calculated by removing the linear trend of each calendar month and monthly climatology from 1950 to 2005. The first and second EOF modes of monthly Indian Ocean SST anomaly are identified as the IOBW and IOD modes which account for 33.6 and 13.4 % of total variance, respectively (Fig. 1).

The observed IOBW mode has a maximum variance at February and a minimum at September with major spectral peaks at 1.5 and 2.5 year. It is conventionally considered as remotely forced mode by ENSO and has positive SST anomaly over the whole Indian Ocean including strong signal in the central Indian Ocean and South China Sea (Fig. 1a). It is similar to the linear trend of annual mean SST but the IOBW has north–south elongated pattern while the linear trend has east–west pattern (not shown).

The observed IOD mode has a maximum variance at September and a minimum variance at April with major spectral peaks at 2–3 and 5 years. The positive phase of IOD mode has dipole structure with a negative core in the eastern Indian Ocean and a positive core in the western Indian Ocean and is considered as an intrinsic mode of Indian ocean–atmosphere coupled system.

Figures 4 and 5 show the simulated first and second mode, respectively, by all models and selected best five models' CMM based on the PCC between the observed and simulated mode. How to select the best models will be explained in Sect. 3.4 in detail. The majority of models can reproduce the observed IOBW mode with high fidelity (Fig. 4). Especially, the BCC-CSM1.1, GFDL-CM3, GISS-E2-R, IPSL-CM5A-LR, and MRI-CGCM3 well display the maximum core on the central/western Indian Ocean and relatively homogeneous feature of the IOBW mode. Some of models show strong east–west gradient with its maximum on either the western Indian Ocean (e.g. ACCESS1-0, HadGEM2-ES, IPSL-CM5A-MR, MPI-ESM-LR) or eastern Indian Ocean (e.g. CNRM-CM5, FGOALS-g2). One model, INM-CM4, has a difficulty in representing IOBW mode. The poor performance of INM-CM4 in representing IOBW mode is mainly contributed by the failure of ENSO simulation. This model seems to simulate weak air-sea interaction, and weak Indian Ocean variability (Du et al. 2013). The models also well capture the seasonal cycle of monthly variance of the first PC with a maximum at February and a minimum at September (Fig. 9c). In addition, the observed spectral peaks at 1.5 and 2.5 are well captured by models (Fig. 10c). The seasonal cycle of PC variance and power spectra in model simulation will revisit at Sect. 4.

In case of the IOD mode, most of models can also reproduce the zonal dipole pattern of IOD mode (Fig. 5). The CNRM-CM5, GFDL-ESM2 M, MIROC5, MPI-ESM-LR, and MRI-CGCM3 are selected as best models for IOD mode in terms of pattern correlation coefficients between observation and simulation. In several models

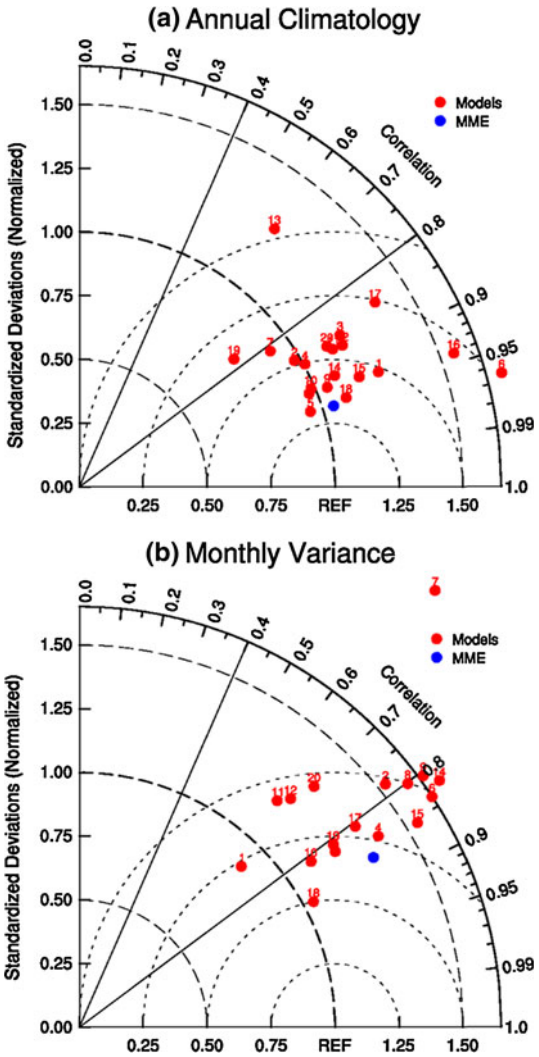

Fig. 3 Performance of 20 models and their MMM in simulating **a** annual mean SST climatology and **b** variance of monthly SST variability over the Indian Ocean (20°S–20°N, 40°–120°E) in terms of Taylor diagram

(e.g., CanESM2, GISS-E2-R, INM-CM4, IPSL-CM5A-LR, IPSL-CM5A-MR and MIROC-ESM) the eastern pole of IOD is not located in the southern coasts of Java and Sumatra, indicating biases in simulating the upwelling in these models (Fig. 5). Some of models such as GISS-E2-R and MIROC-ESM display meridional dipole pattern rather than zonal dipole pattern indicating that the representation of IOD mode is still model-dependent. Most of models realistically capture the seasonal cycle of monthly variance of the second PC with a maximum at September–October and a minimum at April–May but tend to overestimate the amplitude of seasonal cycle (Fig. 9b). In addition, most of models tend to have longer period than observation, having a major spectral peak at 3.5 and a minor peak at 2.5.

Figure 6 is the performance of 20 models and their MMM in capturing spatial distribution of EOF first and second modes in terms of the PCC and Normalized Root Mean Square Error (NRMSE). The individual models have PCC from 0.82 to 0.96 for the IOBW mode except for INM-CM4. The PCC for IOD mode have range from 0.55 to 0.86 except for three poor models in simulating the spatial pattern of IOD mode, indicating models have more difficulty in capturing the IOD than the IOBW mode. It is noted that there is a strong linear relationship between the PCC and NRMSE for the IOBW mode but not for the IOD mode.

3.4 Best model selection

Taking into account the significant inter-model spread over their MMM, efforts have been made to optimally select some of best models in reproducing Indian Ocean SST during historical run period for the sake of more reliable MMM construction and future projection. Firstly, as a representation of EOF modes, we combined the PCCs of the first two EOF modes of SST by weighting with their fractional-variance contributions as below.

$$(combined\,EOF) = (fric\_vari_1) \times (EOF_1) + (fric\_vari_2) \times (EOF_2)$$

Then we assumed that the best model in simulating Indian Ocean SST variability is the model which realistically represent annual mean climatology, monthly variance, and combined EOF together. Therefore, total combined skill is constructed by weighted PCC of annual mean climatology, monthly variance and combined EOF as below.

$$(total\,combined\,skill) = 0.25 \times (Ann.Mean) + 0.25 \times (Mon.Vari.) + 0.5 \times (Comb.EOF)$$

As shown in Fig. 6, the skill of best five models (B5CMM) is better than or comparable with the 20-model's MMM but has much less uncertainty in capturing the IOBW and IOD modes. The selected best five models in representing Indian Ocean SST variability are CNRM-CM5, GFDL-CM3, GISS-E2-R, IPSL-CM5A-LR, and MPI-ESM-LR. To quantitatively represent future changes in Indian Ocean SST variability, we replace all models' MMM to the best five models' MMM (B5MMM) hereafter.

4 Future change

4.1 Annual mean, variance

This section discusses future change of Indian Ocean SST by comparing climatological means and monthly variance

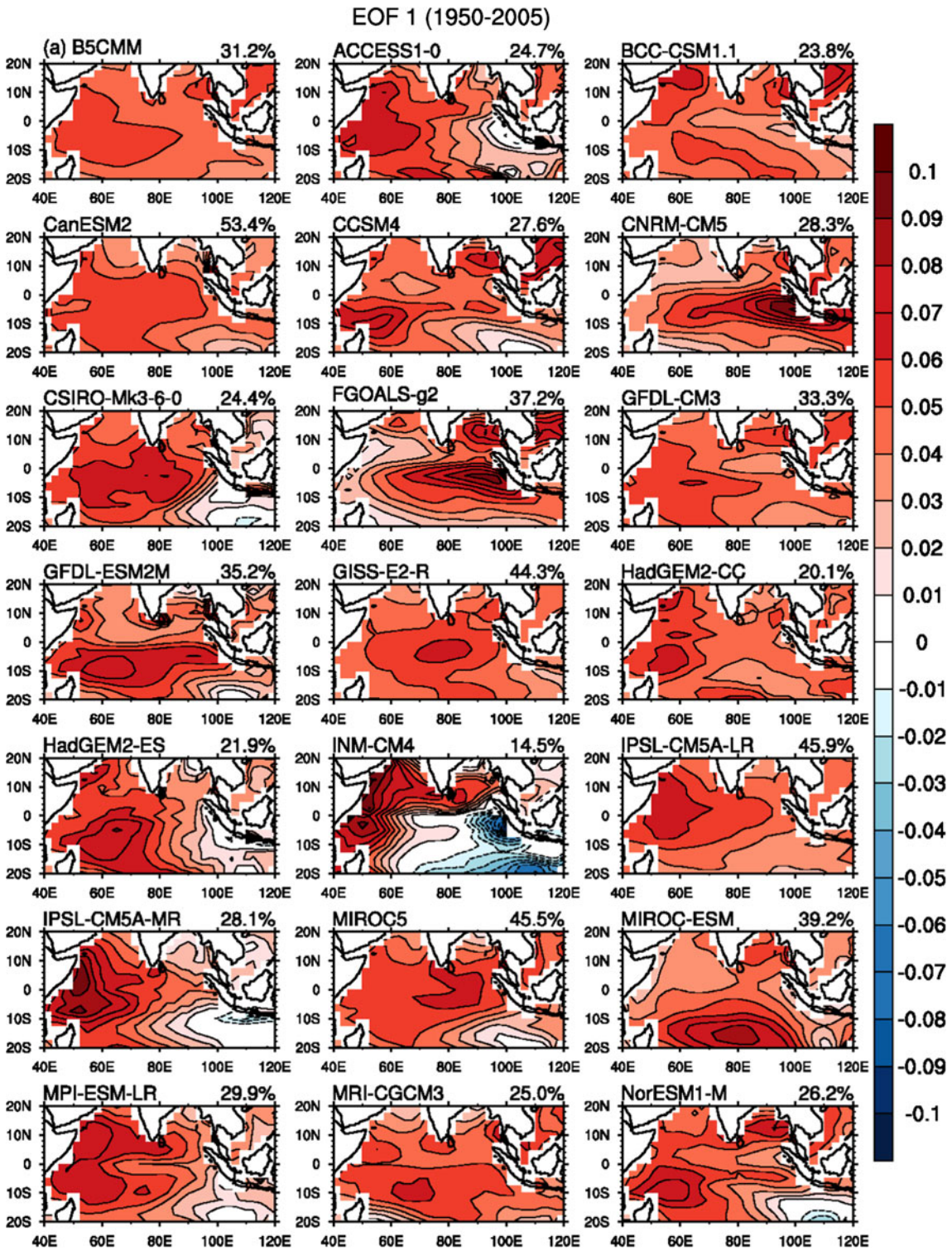

Fig. 4 Spatial distribution of the EOF1 obtained from the five best models CMM (**a**) and individual models (others)

during the historical run period (1950–2005) and the RCP 4.5 run period (2050–2099) using the B5MMM selected in Sect. 3.

Figure 7 shows the difference in annual mean climatology and monthly variance between historical and RCP4.5 runs. The stippling denotes area where the magnitude of MMM exceeds one standard deviation of inter-model spread. It is meaningful to note whether the magnitude of the change exceeds the uncertainty measured by the standard deviation of inter-model spread against the

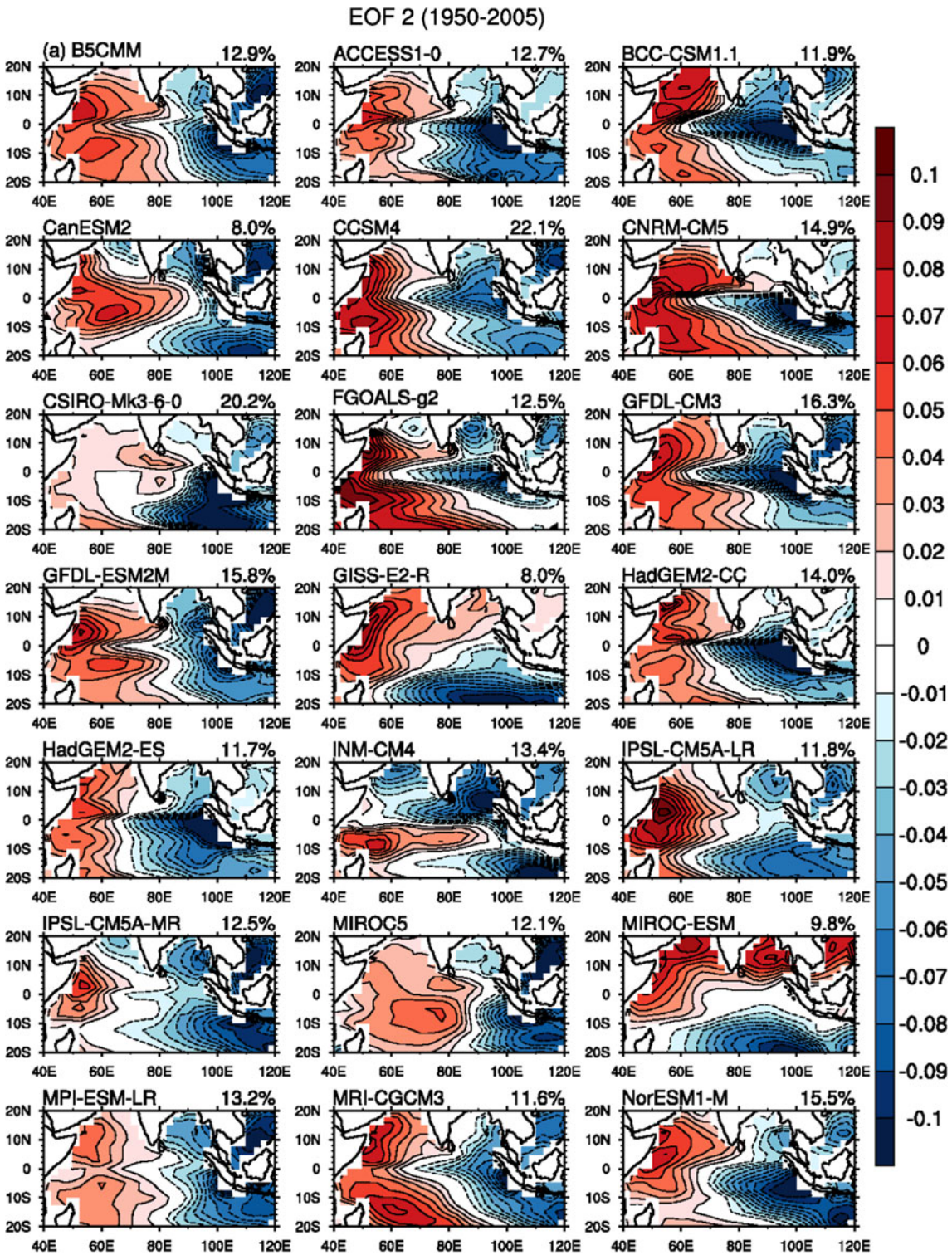

Fig. 5 Spatial distribution of the EOF2 obtained from the five best models CMM (**a**) and individual models (others)

B5MMM. Both all MMM and B5MMM consistently represent strong warming over the whole tropical Ocean (Fig. 7a, b). The changes in mean climatological SST display IOD-like pattern over the Indian Ocean with enhanced warming in the northwestern Indian Ocean and relatively weaker warming off the Sumatra–Java coast (this pattern is similar to Zheng et al. 2013). Meanwhile, large SST warming is also located in the eastern tropical Pacific

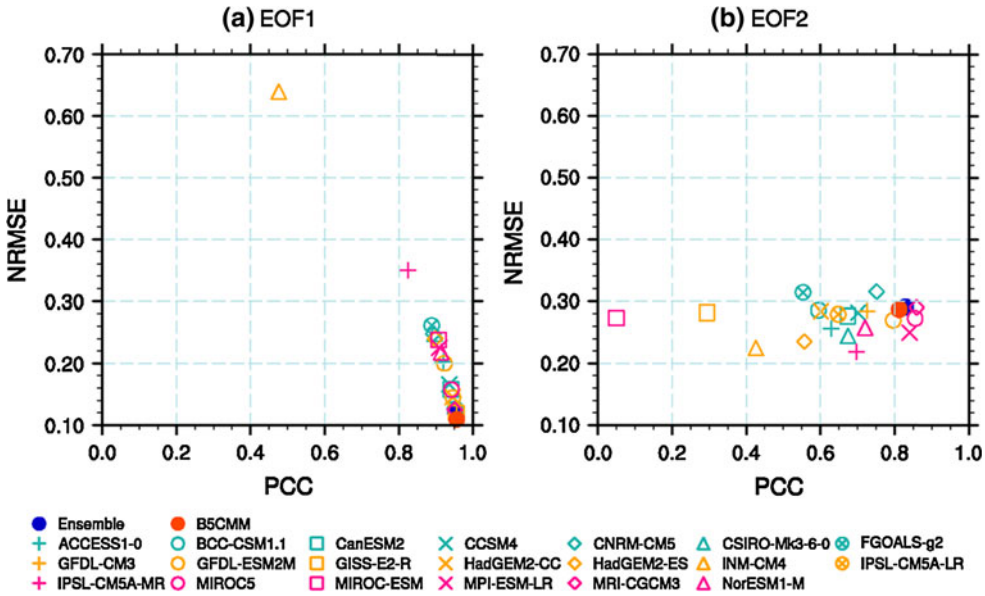

Fig. 6 Performance of 20 models and their MMM in capturing spatial distribution of the **a** EOF1 and **b** EOF2 in terms of scatter diagram between pattern correlation coefficients and normalized RMSE

with El-Nino-like warming pattern indicating the tropical thermocline shoaling and Walker circulation weakening. The IOD-like and El-Nino-like warming are consistent in both all MMM and B5MMM. It is also noted that the monthly SST variance is increased over the eastern and southwestern Indian Ocean (Fig. 7c, d). On the other hand, there is a big difference between all MMM and B5MMM in displaying changes in monthly variance over the eastern Pacific (Fig. 7c, d). No prominent or slightly reduced variance can be found over the eastern Pacific in all MMM while B5MMM shows increased monthly variance over the tropical central to eastern Pacific. It indicates that best models selected by the performance in representing Indian Ocean SST variability are characterized by the models that simulating increased ENSO activity. Therefore, mean state change under global warming has IOD (El Nino)-like pattern over the equatorial Indian (Pacific) Ocean. However, it is hard to conclude that El Nino activity will increase in the future projection because the magnitude of change does not exceed the uncertainty measured by the standard deviation of inter-model spread.

4.2 The IOBW and IOD modes

Changes in the mean states may affect the IOBW and IOD modes since a greater amount of warming in the Indian Ocean can amplify the SST variability through enhanced air-sea coupled processes (Choi et al. 2009). This subsection discusses how the IOBW and IOD modes would change in terms of their percentage variance, seasonal cycle, major periodicity, and spatial distribution under the anthropogenic global warming using the selected best five models. As mentioned in Sect. 2, the EOF analysis is applied to the best five models' consecutive multi-model (B5CMM) data for identifying the future (2050–2095) IOBW and IOD modes in the models.

First, we investigate changes in the percentage variance for which are accounted by the two dominant modes in the

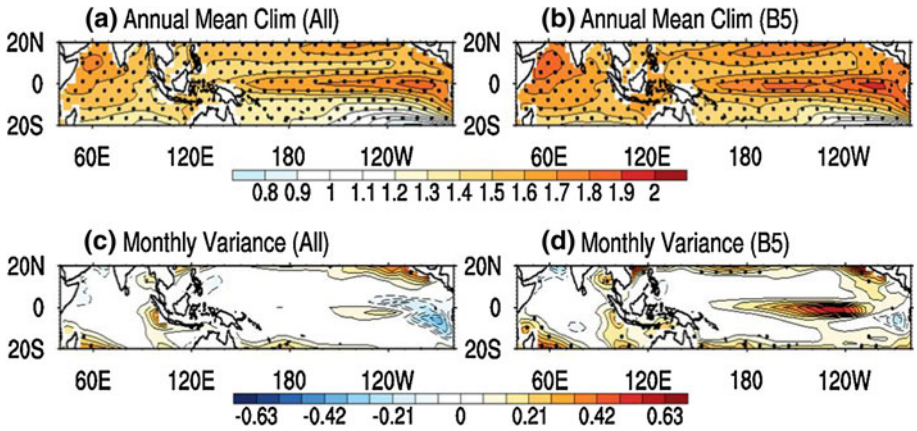

Fig. 7 Change of **a**, **b** annual mean SST climatology and **c**, **d** variance of monthly SST using the all model's MMM (**a**, **c**) and the B5MMM (**b**, **d**). Changes are given for the RCP 4.5 simulation for the period 2050 to 2099 relative to historical simulation for the period 1950 to 2005 in CMIP5. *Stippling* denotes areas where the magnitude of the B5MMM exceeds the standard deviation of inter-model spread

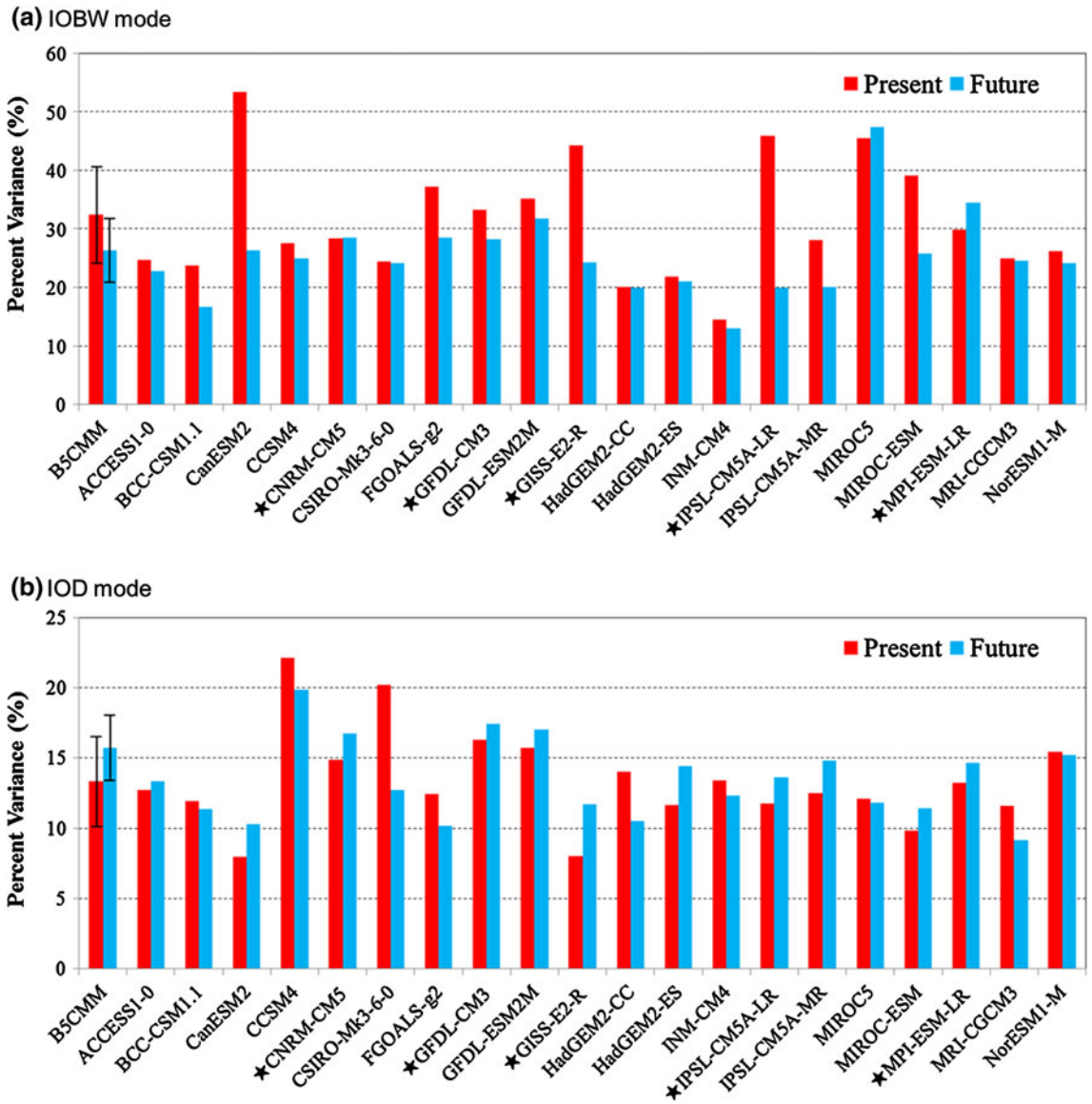

Fig. 8 Change in the percentage variance of **a** the IOBW mode and **b** the IOD mode in individual models and B5CMM. The *vertical error bars* denote the standard deviation of inter-model variability associated with best five models

Indian Ocean variability. Figure 8 displays the percent variance of each mode by individual models along with those of the B5CMM. Although there is apparent inter-model spread, most of models reasonably represent the percent variance of the IOBW and IOD modes in the present climate. It is found that the variance of IOBW mode will weaken considerably by 6.1 % from 34.5 to 26.4 in the B5CMM, in spite the fact that the annual mean climatological is expected to be increased. In addition, 17 out of 20 coupled models project the decrease of the IOBW's variance in future (Fig. 10a). On the other hand, the IOD mode will be maintained or slightly intensified by 2.4 % from 13.3 to 15.7 in the B5CMM (Fig. 8b). 11 out 20 models predict the intensification indicating uncertainties among the models. This result is consistent with Zheng et al. (2013). They argued that the response of IOD intensity to global warming is mainly controlled by the local oceanic dynamics, the thermocline shoaling in the eastern Indian Ocean in particular. They also mentioned that the IOD activity does not intensified in spite of enhanced thermocline feedback since the cancelling out with weakened atmospheric feedback.

Second, the B5CMM tends to project amplification of seasonal cycle of monthly variance of both modes shown in Fig. 9. That is, the IOBW (IOD) mode may have stronger variance during February (September and October) in future than present while the two modes will have much reduced variance during low seasons in future.

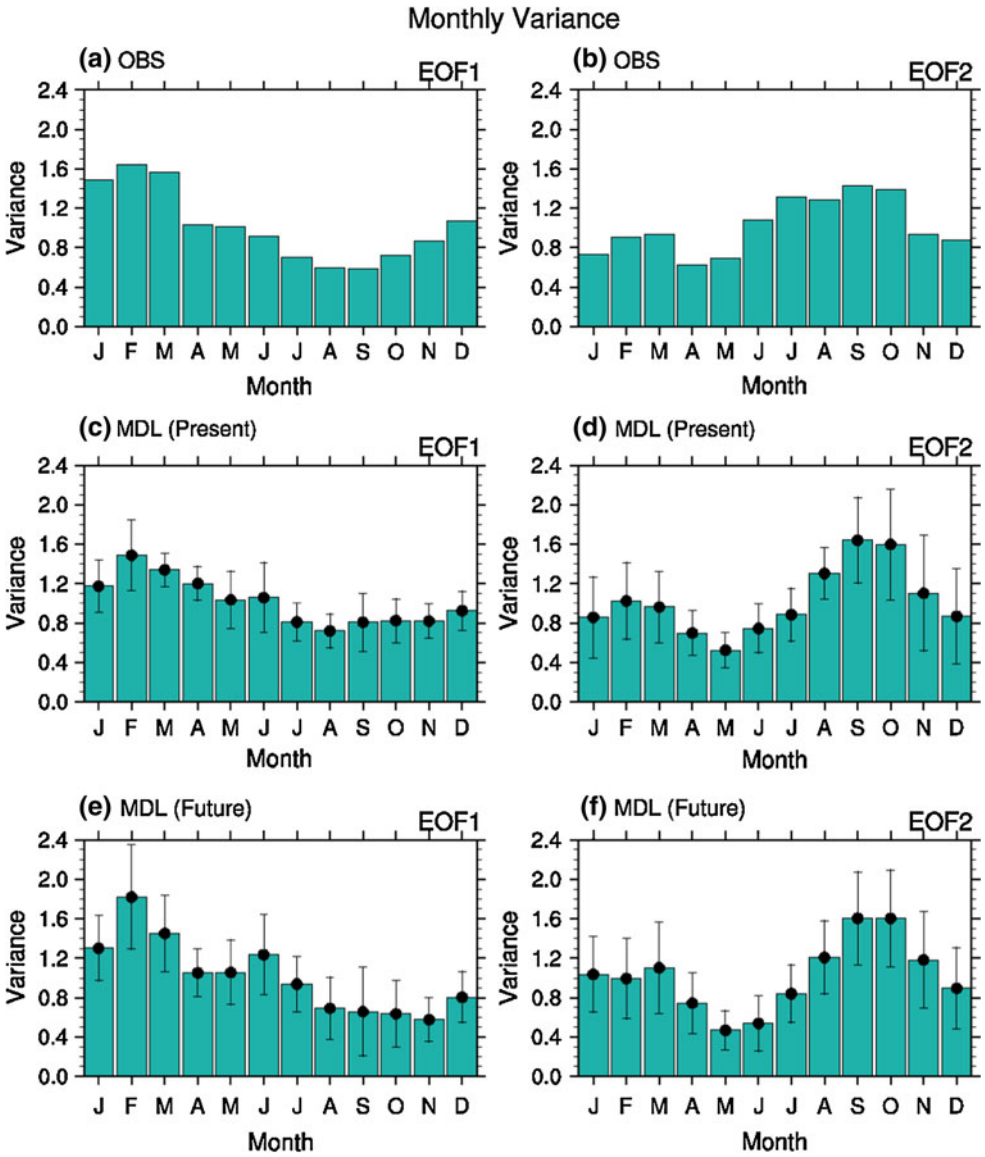

Fig. 9 Ensemble mean monthly standard deviation of normalized PC derived from **a** observation, **b** historical simulation (1950–2005) and **c** future projection (2050–2099). *Error bar* denote the standard deviation of inter-model variability

In particular, comparison between the Fig. 9c and e indicates that the reduction of significant percentage variance of the IOBW is mainly attributable to the decrease of the variance of the IOBW mode during late summer and fall.

Third, there will be changes in dominant frequency of variability of the two modes (Fig. 10). It is well recognized that the IOBW mode has spectral peak around 2.5–3 years in observation related to the quasi-biennial variability of ENSO. The B5CMM also captures the significant periodicity peaking at 2.5–3 years in present although it tends to underestimate the spectral power. The models' notable bias in the power spectrum is considerable overestimation of spectral power longer than 4 years. In future, the best models tend to project enhancement of the IOBW variability on 2.5–3-year time scale related to ENSO in spite of the fact that the total variance of the IOBW is expected to be considerably reduced. It is noted that the major periodicity of the IOD, the intrinsic coupled mode, in the coupled models (Fig. 10d) are considerably different from the observation (Fig. 10b). The CMIP5 coupled models tend to have longer time scale of the IOD than the observation. In future projection, the IOD mode may have shorter time scale than in present (Fig. 10f). Further study is needed to better understand why the major periodicity of the IOD mode is shifted to shorter time scale under global warming scenario in the coupled models.

Finally, we investigate changes in spatial distributions of the two modes. Figures 11 and 12 show the spatial distribution of the first two EOF modes in the future (2050–2099) projected by individual models and the B5CMM. It is found that the coupled models tend to predict notable changes of spatial pattern in the IOBW but not in the IOD mode. In future, the IOBW mode may have less homogeneity in their basin-wide warming pattern (Fig. 11)

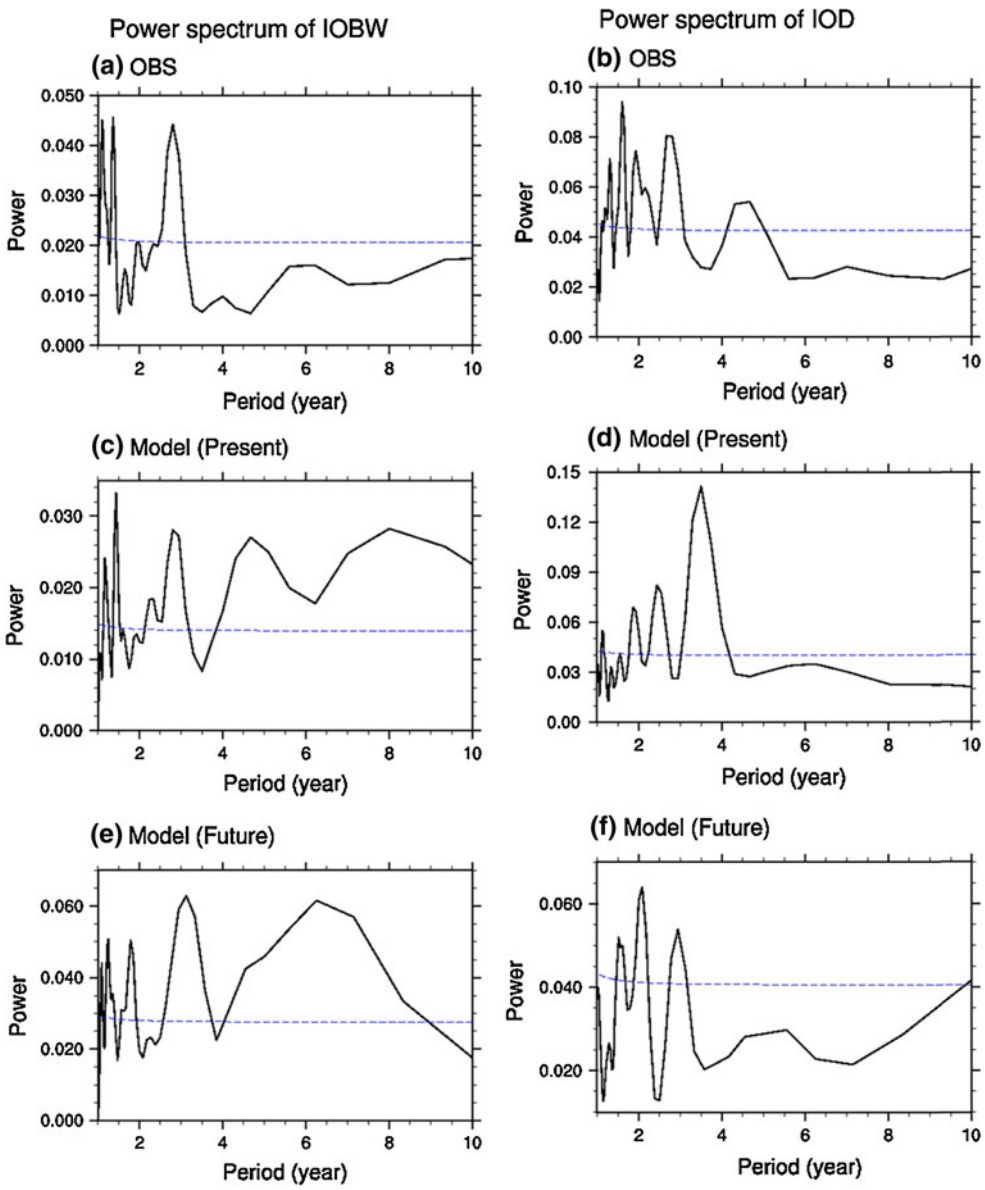

Fig. 10 Power spectrum of PC time series from observation (**a**, **b**) and B5MMM for the present simulation (**c**, **d**) and future projection (**e**, **f**). *Blue dotted line* indicates the red noise

than in present (Fig. 4). In particular, the change is notable over the eastern Indian Ocean for the IOBW mode. Differently from the IOBW mode, the dipole pattern in the IOD mode exhibiting positive anomaly over the northwest Indian Ocean and negative core over on the southeastern Indian Ocean (Fig. 12) is analogous to that of present climate (Fig. 5). Someone may argue whether that the IOBW mode can still be represented by EOF first mode in the future projection. To demonstrate this argument, we calculated the ENSO-regressed Indian Ocean SST, and found the consistency between ENSO-regressed SST pattern and EOF first mode both in historical and future projection (figure not shown). Several models (CCSM4, GFDL-CM3, GFDL-ESM2 M, IPSL-CM5A-MR, NorESM1-M) have cold biases in the ENSO-regressed field over the eastern Indian Ocean, but the maximum positive region is consistent with that of EOF first mode. The INM-CM4 which showed poor performance in representing IOBW mode seems to be mainly contributed by the failure of ENSO simulation. In the future projection, homogeneity is also reduced in the ENSO-regressed pattern in the most of models as described in EOF first mode indicating that EOF first mode can be used to examine IOBW mode under the global warming.

4.3 Changes in the ENSO–IOBW relationship

In the previous section, we discussed how the IOBW and IOD would change in terms of percent variance, seasonal cycle, periodicity, and horizontal patterns. It was found that in spite of amplified seasonal cycle and dominant frequency, the percent variance of IOBW will decrease with spatially

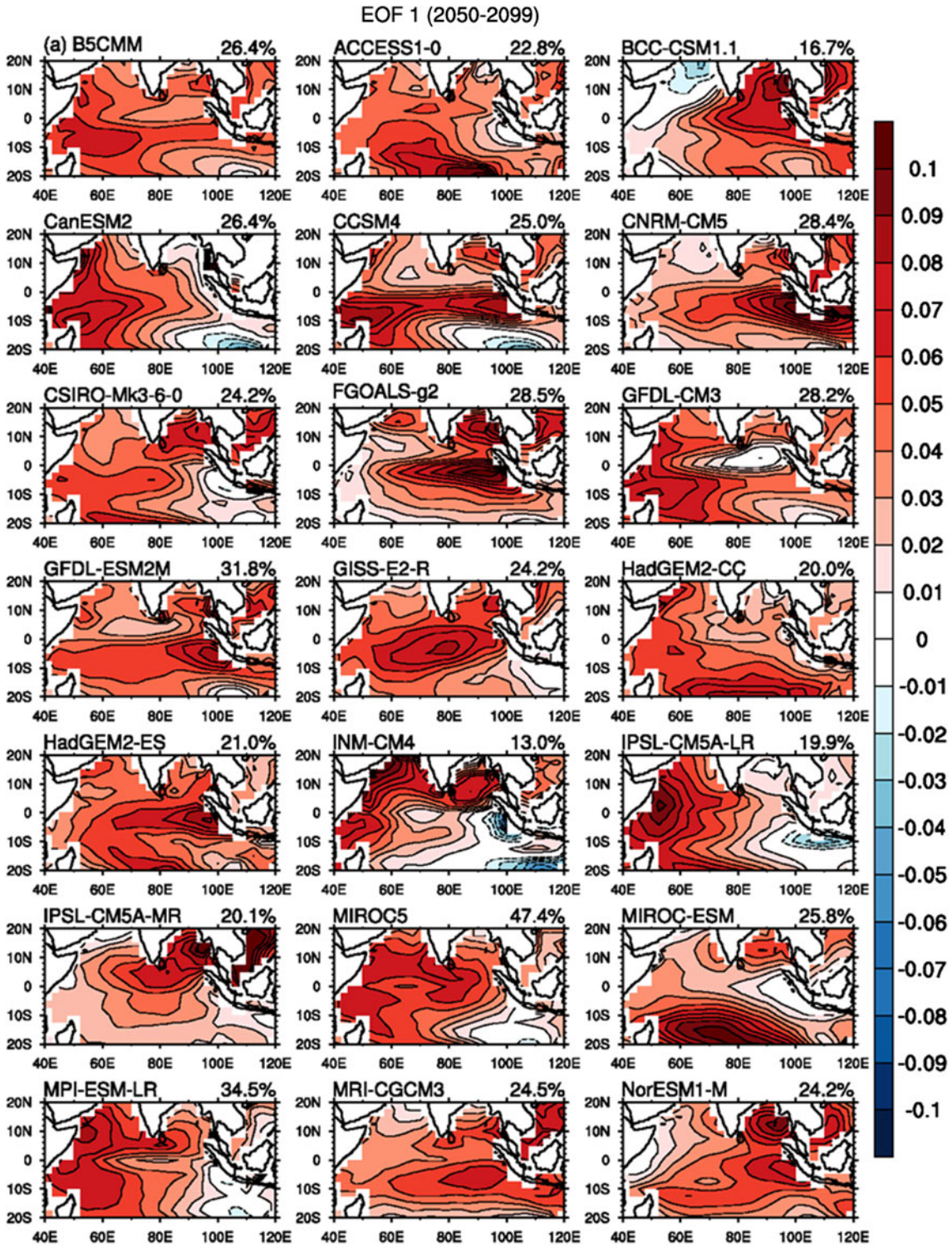

Fig. 11 Spatial distribution of the EOF1 obtained from the B5CMM and individual models from 2050 to 2099

inhomogeneous warming pattern. Except for several models, the IOBW mode can still be represented by EOF first mode on account of the consistency between ENSO-regressed pattern and the EOF first mode. Then, are there any changes in IOBW–ENSO relationship? Thus, this subsection is devoted to the investigation of future changes in the ENSO–IOBW relationship. Recently, several papers have touched on the features of the CMIP5 models. Kug et al. (2012) and Kim and Yu (2012) demonstrated that the CGCMs in the CMIP5 have slightly better performance in

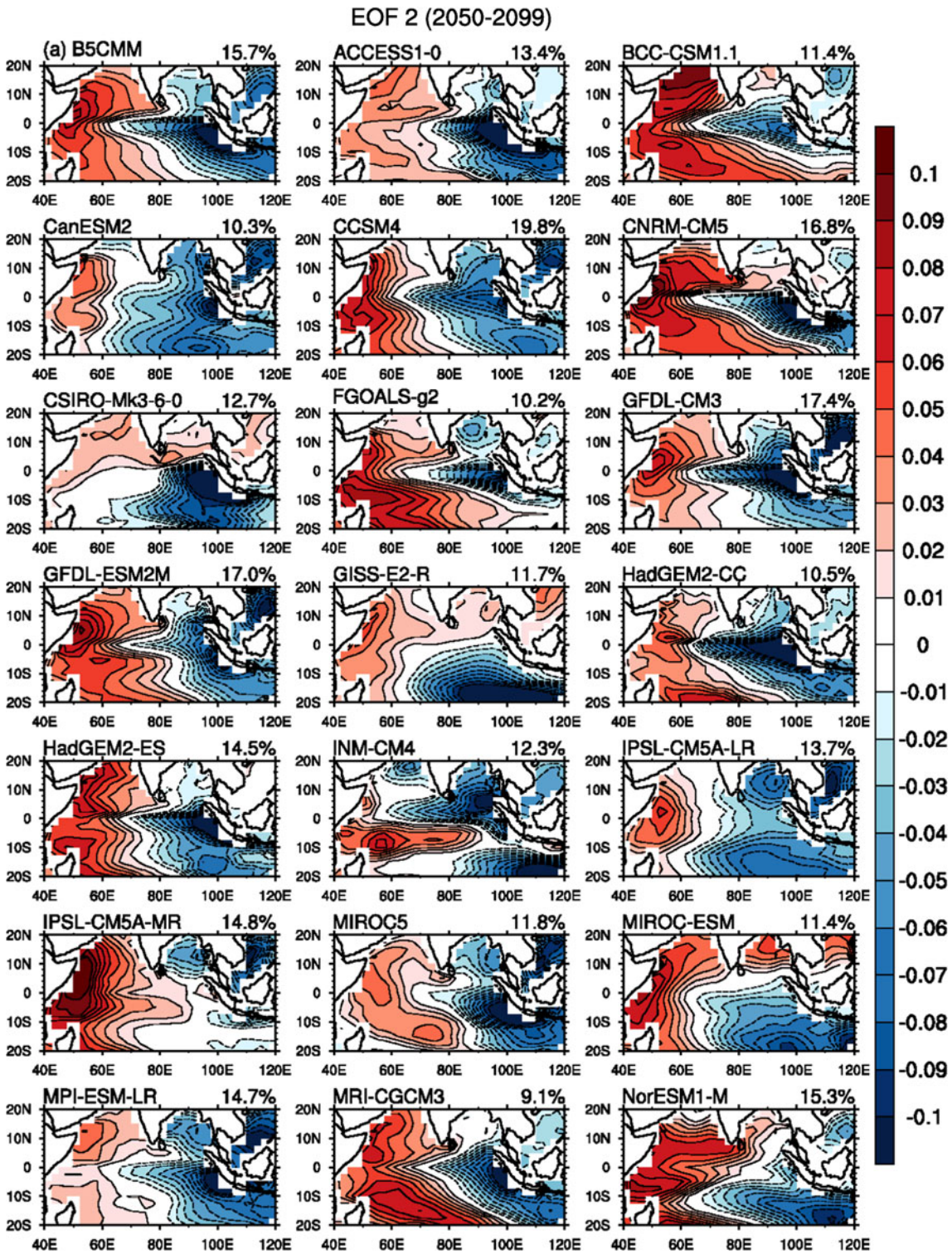

Fig. 12 Same as in Fig. 13 except for the EOF2

simulating the two types of El Niño event independently compared to those in CMIP3. Yeh et al. (2012) have shown that the CMIP5 models tend to simulate the pattern of tropical warming as El Niño-like structure and such changes give rise to a center of action associated with the ENSO amplitude had shifted to the east. It can be expected that such changes may be accompanied by changes in ENSO-Indian Ocean relationship because the IOBW which is regarded as passive mode of ENSO would be significantly affected by the Pacific Ocean mean state and variance change.

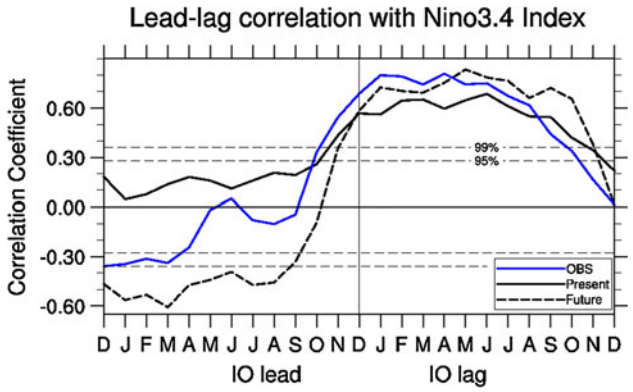

Fig. 13 Lead-lag relationship between the PC time series of B5MMM equivalent to IOBW mode and DJF Nino3 index derived from observation (*blue line*), and simulation based on B5MMM for the historical (*black solid line*), and future (*black dotted line*) periods

In fact, the amplified seasonal cycle and dominant frequency of IOBW should be accompanied with increased temporal relationship between ENSO and IOBW. As a representation of ENSO activity, Nino3.4 index is calculated by averaging SSTs over the east central tropical Pacific (5 N:5 S, 170:120 W). Figure 13 displays the lead-lag relationship between boreal wintertime (DJF) Nino3.4 index and the PC time series equivalent to the IOBW mode. In observation, Indian Ocean warming is always followed by with preceding wintertime El Niño peaking in spring and this positive relationship is maintained until summer and abruptly decayed during fall season. The B5MMM is able to capture the relationship with a high fidelity but tends to underestimate the observed relationship between Indian Ocean and wintertime El Niño during spring and summer. In particular, the B5MMM much better simulate it than the all models' MMM (figure not shown). In the future, lagged correlation between the IOBW mode and wintertime ENSO will increase in general which may be related to the strengthening of dominant frequency coincide with ENSO periodicity.

The increased temporal relationship between ENSO and IOBW can't support the decrease in IOBW variance. Then we might expect that the spatially inhomogeneous Indian Ocean warming pattern may lead to decrease in IOBW variance. In this sense, we try to answer the reason for reduced variance by examining the changes in ENSO impact on Indian Ocean SST. In order to assess the changes in the impact of ENSO on Indian Ocean, Fig. 14 describes the correlation coefficients between DJF Nino3.4 index and atmospheric circulation fields for present climate and future projection. The B5MMM realistically represent the atmospheric response to external forcing (i.e., El Nino) with the southern oscillation pattern and enhanced (suppressed) precipitation anomalies over the central (western) Pacific during the historical simulation (Fig. 14a). In the future projection, the relationship between boreal wintertime eastern Pacific SST variability and western Pacific circulation field is strengthened indicating the increased atmospheric teleconnection in response to El Nino (Fig. 14b). It is further illustrated in Fig. 14c, d. Striking feature is the strong easterly anomalies along the equatorial Indian Ocean in the future projection. The strong easterly induced by El Nino derives the surface cooling through evaporation, coastal upwelling and vertical mixing over the tropical eastern Indian Ocean. This enhanced air-sea coupling system in the Indian Ocean is similar to positive IOD structure (Yu et al. 2002). Another interesting feature is found over the western north Pacific SST. The cold SST located at the western North Pacific could feed back to western North Pacific subtropical high (WNPSH) and the WNPSH, in turn, can intensify cooling over that region.

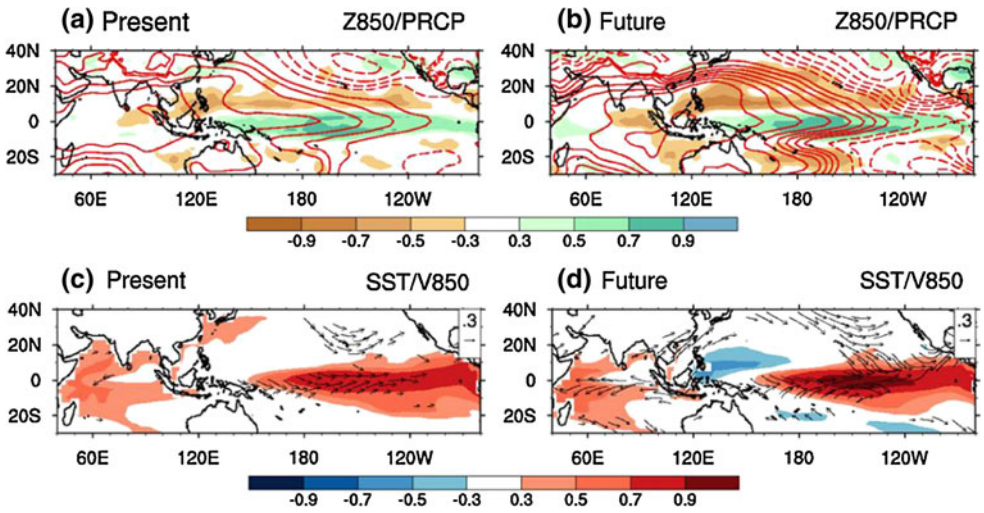

Fig. 14 Spatial pattern of the correlation coefficients with DJF Nino3.4 index for present climate (*left*) and future projection (*right*) derived from B5MMM. *Upper panel* is for DJF 850-hPa geopotential height (contour), precipitation (*shading*) while *lower panel* is for SST (*shading*) and 850-hPa wind (*vector*) with correlations significant at 95 % confidence ($r > 0.3$)

Therefore, the enhanced air-sea coupling over the Indian-western Pacific climate in response to El Nino activity in the future projection make favorable condition for positive IOD while it deriving relatively cold temperature over the eastern Indian Ocean. Finally, this positive IOD-like ENSO response weaken the relationship between eastern Indian Ocean and El Nino while strengthen the relationship with western Indian Ocean. Although this study does not consider the changes in El Nino characteristics under global warming, the lead-lag relationship between ENSO and IOBW before ENSO mature phase is significantly negatively increased. It may be related to the strong biennial coupling between Indian Ocean and Pacific Ocean. It should be mentioned that the enhanced easterly anomaly over the eastern Indian Ocean shows similar structure even using different ENSO indices (i.e., Nino3 and Nino4 indices). The strengthened atmospheric circulation and precipitation in response to El Nino is also consistent in all MMM (figure not shown).

On the contrary to the IOBW–ENSO relationship, the IOD does not show any significant change in their lead-lag relationship with ENSO (not shown). Therefore, changes in IOD variability under global warming is not from external forcing but mainly controlled by local dynamics. It is consistent with the results from Zheng et al. (2013) indicating that recent changes in the IOD mode are likely due to natural variations.

5 Summary

We investigate the future changes of the Indian Ocean basin-wide (IOBW) and dipole (IOD) modes projected by 20 coupled models that participated in the phase five of the Coupled Model Intercomparison Project (CMIP5) by comparing two runs: the historical run under changing solar-volcanic forcing and anthropogenic influences from 1850 to 2005 and the RCP 4.5 run assuming that radiative forcing will stabilize at about 4.5 Wm^{-2} after 2100. A metric for evaluation of the model's performance is designed to select a subset of models. The five best models' MMM (B5MMM) has a higher skill for the Indian Ocean metrics with better representation of the IOBW and IOD modes in their spatial distribution, seasonal cycle, major periodicity, and relationship with ENSO. The future changes in the Indian Ocean mean state and the two major modes are summarized as follows.

The changes in mean climatological SST display positive IOD-like pattern over the Indian Ocean with enhanced warming in the northwestern Indian Ocean and relatively weaker warming off the Sumatra–Java coast (this pattern is similar to Zheng et al. 2013). Meanwhile, large SST warming is also located in the eastern tropical Pacific with El-Nino-like warming pattern indicating the tropical thermocline shoaling and Walker circulation weakening. It is also noted that the monthly SST variance is increased over the eastern and southwestern Indian Ocean (Fig. 7c, d).

We also discussed how the IOBW and IOD modes would change in terms of their percentage variance, major periodicity, and spatial distribution under the anthropogenic global warming using the selected best five models. Analysis of the B5CMM revealed that in spite of amplified seasonal cycle and dominant frequency, the percent variance of IOBW will decrease by 6.1 % from 34.5 to 26.4 % with spatially inhomogeneous warming pattern. We concluded that decrease in IOBW variance is result from changes in ENSO impact on Indo-western Pacific climate. In the future projection, strong easterly anomalies along the equatorial Indian Ocean induced by El Nino derives the surface cooling through evaporation, coastal upwelling and vertical mixing over the tropical eastern Indian Ocean. This enhanced air-sea coupling system is similar to positive IOD structure. Therefore, the enhanced air-sea coupling over the Indian-western Pacific climate in response to El Nino activity in the future projection make favorable condition for IOD while it deriving relatively cold temperature over the eastern Indian Ocean. Finally, this positive IOD-like ENSO response weaken the relationship between eastern Indian Ocean and El Nino while strengthen the relationship with western Indian Ocean.

The IOD mode, on the other hand, the intrinsic coupled mode of Indian Ocean variability, may not be changed appreciably under the anthropogenic global warming. The coupled models project slight increase of its total variance by 2.4 % but the model spread for the projection is large. Its spatial distribution and relationship with ENSO will not be changed significantly. However, the model projections show significant shift of major periodicity of the IOD mode variability from 3–4 years to 2–3 years. Further study is needed to understand why the major periodicity of the model's intrinsic coupled mode would be changed under the global warming.

This study shows capability of the coupled modeling in simulating the Indian Ocean mean state and variability in the CMIP5 models. However, we still identify considerable biases of model's simulation over the Indian Ocean. A notable bias is that more than half of the CMIP5 coupled models have difficulty in capturing the spatial distribution of the IOD mode, particularly over the equatorial Indian Ocean. Some models tend to have negative anomaly extended far west along the equator in the positive phase of the IOD. Few models rather have the north–south dipole than the east–west. Understand of the models' deficiencies are of importance for more reliable estimation of the future change of the Indian Ocean variability.

Acknowledgments This work was supported by the National Research Foundation of Korea (NRF) through a Global Research Laboratory (GRL) Grant (MEST 2011-0021927) and IPRC, which is in part supported by JAMSTEC, NOAA, and NASA. Jung-Eun Chu is supported by NRF of Korea through Fostering Core Leaders of the Future Basic Science Program. We acknowledge the World Climate Research Programme's Working Group on Coupled Modeling, which is responsible for CMIP, and we thank the climate modeling groups listed in Table 1 of this paper for producing and making available their model output. For CMIP the U.S. Department of Energy's Program for Climate Model Diagnosis and Intercomparison provides coordinating support and led development of software infrastructure in partnership with the Global Organization for Earth System Science Portals. This is the SOEST publication number 9015 and IPRC publication number 1020.

References

Abram NJ, Gagan MK et al (2008) Recent intensification of tropical climate variability in the Indian Ocean. Nat Geosci 1:849–853

Alory G, Wijffels S, Meyers G (2007) Observed temperature trends in the Indian Ocean over 1960–1999 and associated mechanisms. Geophys Res Lett 34:L02606. doi:10.1029/2006GL028044

Choi J, An S-I, Dewitte B, Hsieh WW (2009) Interactive feedback between the tropical Pacific decadal oscillation and ENSO in a coupled general circulation model. J Climate 22:6597–6611

Chowdary JS, Xie SP, Lee JY, Kosaka Y, Wang B (2010) Predictability of summer Northwest Pacific climate in 11 coupled model hindcast: local and remote forcing. J Geophys Res-Atmos 115:D22121. doi:10.1029/2010JD014595

Chowdary JS, Xie S-P, Tokinaga H, Okumura YM, Kubota H, Johnson NC, Zheng X-T (2012) Inter-decadal variations in ENSO teleconnection to the Indo-western Pacific for 1870–2007. J Climate 25:1722–1744

Du Y, Xie S-P (2008) Role of atmospheric adjustments in the tropical Indian Ocean warming during the 20th century in climate models. Geophys Res Lett 35:L08712. doi:10.1029/2008GL033631

Du Y, Xie S-P, Yang Y-L, Zheng X-T, Liu L, Huang G (2013) Indian ocean variability in the CMIP5 multimodel ensemble: the basin mode. J Clim 26:7240–7266

Giannini A, Saravanan R, Chang P (2003) Oceanic Forcing of Sahel Rainfall on Interannual to Interdecadal Time Scales. Science 302(5647):1027–1030

Hsu P, Li T (2012) Is "rich-get-richer" valid for Indian Ocean and Atlantic ITCZ? Geophys Res Lett 39:L13705. doi:10.1029/2012GL052399

Ihara C, Kushnir Y, Cane MA (2008) Warming trend of the Indian Ocean SST and Indian Ocean dipole from 1880 to 2004. J Climate 21:2035–2046

Kalnay E (1996) The NCEP/NCAR 40-year reanalysis project. Bull Am Meteor Soc 77:437–471

Kim ST, Yu JY (2012) The two types of ENSO in CMIP5 models. Geophys Res Lett 39:L11704

Kug JS, Ham YG, Lee JY, Jin FF (2012) Improved simulation of two types of El Niño in CMIP5 models. Environ Res Lett 7:034002. doi:10.1088/1748-9326/7/3/034002

Latif M, Barnett TP (1995) Interactions of the tropical Oceans. J Climate 8:952–964

Lee JY, Wang B (2012) Future change of global monsoon in the CMIP5. Clim Dyn. doi:10.1007/s00382-012-1564-0. (in press)

Lee JY, Wang B, Kang IS, Shukla J et al (2010) How are seasonal prediction skills related to models' performance on mean state and annual cycle? Clim Dyn 35:267–283

Luo JJ, Sasaki W, Masumoto Y (2012) Indian Ocean warming modulates Pacific climate change. PNAS. doi:10.1073/pnas.1210239109. (in press)

Meehl GA, Covey C, Delworth T, Latif M et al (2007a) The WCRP CMIP3 multi-model dataset: a new era in climate change research. Bull Am Meteor Soc 88:1383–1394

Meehl GA, Stocker TF, Collins WD et al (2007b) Global climate projection. In: Solomon S, Qin D, Manning M et al (eds) Climate change 2007: the physical science basis. Contribution of working group I to the fourth assessment report of the intergovemmental panel on climate change. Cambridge University Press, Cambridge

Rayner N et al (2003) Global analyses of sea surface temperature, sea ice, and night marine air temperature since the late nineteenth century. J Ceophys Res 108:4407. doi:10.1029/2002JD002670

Saji NH, Yamagata T (2003) Structure of SST and surface wind variability during Indian Ocean dipole mode events: COADS observations. J Climate 16:2735–2751

Saji NH, Goswami BN, Vinayachandran PN, Yamagata T (1999) A dipole mode in the tropical Indian Ocean. Nature 401:360–363

Saji NH, Xie SP, Yamagata T (2006) Tropical Indian Ocean variability in the IPCC twentieth-century climate simulations. J Climate 19:4397–4417

Schott FA, Xie SP, McCreary JP (2009) Indian Ocean circulation and climate variability. Rev Geophys 47:RG1002

Taylor KE, Stouffer RJ, Meehl GA (2012) An overview of CMIP5 and the experiment design. Bull Am Meteor Soc 93:485–498

Tokinaga H, Xie SP, Deser C, Kosaka Yu, Okumura YM (2012) Slowdown of the walker circulation driven by tropical Indo-Pacific warming. Nature 491:439–443

Vecchi GA, Soden BJ (2007) Global warming and the weakening of the tropical circulation. J Climate 20:4316–4340

Wang B, Yim SY, Lee JY, Liu J, Ha KJ (2013) Future change of Asian-Australian monsoon under RCP 4.5 anthropogenic warming scenario. Clim Dyn. doi:10.1007:s00382-013-1769-x

Webster PJ, Moore AM, Loschnigg JP, Leben RR (1999) Coupled ocean-atmosphere dynamics in the Indian Ocean during 1997–1998. Nature 401:356–360

Xie SP, Hu K, Hafner J, Tokinaga H, Du Y, Huang G, Sampe T (2009) Indian Ocean capacitor effect on Indo-western Pacific climate during the summer following El Niño. J Climate 22:730–747

Yeh SW, Ham YG, Lee JY (2012) Changes in the tropical Pacific SST trend from CMIP3 to CMIP5 and its implication of ENSO. J Clim 25:7764–7771

Yu J-Y, Mechoso CR, McWilliams JC, Arakawa A (2002) Impacts of the Indian Ocean on the ENSO cycle. Geophys Res Lett 29(8):1204. doi:10.1029/2001GL014098

Zheng X-T, Xie S-P, Vecchi GA, Liu Q, Hafner J (2010) Indian Ocean dipole response to the global warming: analysis of ocean-atmospheric feedbacks in a coupled model. J Climate 23:1240–1253

Zheng X-T, Xie S-P, Du Y, Liu L, Huang G, Liu Q (2013) Indian Ocean dipole response to global warming in the CMIP5 multi-model ensemble. J Climate. doi:10.1175/JCLI-D-12-00638.1. (in press)